IEEE Access
Multidisciplinary | Rapid Review | Open Access Journal

Received October 19, 2018, accepted November 9, 2018, date of publication December 3, 2018,
date of current version January 16, 2019.

Digital Object Identifier 10.1109/ACCESS.2018.2884637

Synchronous and Asynchronous Radar Interference Mitigation

FARUK UYSAL, (Senior Member, IEEE)
Microwave Sensing, Systems and Signals Group, Faculty of Electrical Engineering, Mathematics and Computer Science, Delft University of Technology, Delft 2628CD, The Netherlands

e-mail: f.uysal@tudelft.nl

ABSTRACT This paper considers the interference mitigation problem for radar systems by focusing on emerging signal separation (decomposition) methods. We define appropriate transform domains to sparsely represent the interference and the signal of interest to separate them from each other. To show the effectiveness of the proposed algorithm at actual radar systems, the method is applied to real data from two different radar systems. The proposed method is applied to an automotive radar to mitigate the asynchronous interference caused by other automotive radars. Following, the proposed method is demonstrated on a polarimetric agile radar for synchronous mutual-interference mitigation. Significant improvements are observed at the signal-to-interference ratio for both radar systems during the course of experiments.

INDEX TERMS Signal separation, interference mitigation, automotive radar, mutual-interference.

I. INTRODUCTION

As the number of sensing devices increases in different application areas such as autonomous driving and internet of things (IoT), the number of radar sensors is also increasing due to their all-weather day and night capabilities. In most cases, these radar sensors must operate in the same or similar frequency band due to spectrum allocation and works in close proximity to other radar and/or transceivers. In such a situation where multiple radars are in close proximity to each other, they start interfering with each other and degrade the quality of operation. Thus, interference mitigation is crucial for uninterrupted and correct information flow from radar sensors.

There are different approaches available in the literature. Such that Fabrizio and Farina [1] proposed a generalized estimation of multipath signals (GEMS) algorithm for blind source separation which estimates the interference waveforms in the same frequency channel as the signal of interest. However, such an approach may not be applicable when there is no multi-path between interferer and the reference radar. In [2] a known type of interference signal's parameters are estimated by using time-modulated windowed all-phase Discrete Fourier transform. Then the estimated signal is exactly reconstructed and eliminated from the original signal. In synthetic aperture radar (SAR) imaging, other methods are present for radio-frequency interference (RFI) and man-made interference (MAI) mitigation such as presented in [3] and [4]. In this paper, unlike the previous approach, we propose to use morphological analysis and signal separation approach to mitigate interference.

In addition to the signal separation methods, there are other methods available in the literature for synchronous and asynchronous interference mitigation which may satisfy real-time processing needs [5]. The basic approach is to remove distorted samples from time domain signals which need precise detection of the affected samples. However, this approach creates ringing artifacts (due to the discontinuity inside the frequency band) or increases sidelobes in range profiles. To avoid any ringing artifacts in the processed radar data, the neighborhood of affected samples may be smoothed using a window function [6]. Alternatively one may fill the gaps with sparsity-based methods or interpolation [7]. Note that, all these methods depend on precise detection of interference location and duration. Moreover, if the duration of interference covers most of the received signal duration, then these methods are not effective. The method proposed in this paper is novel in the sense that it does not need any prior knowledge nor detection of the interference.

Signal separation methods used in radar domain usually concentrate on clutter mitigation. Clutter can be defined as the unwanted radar returns which are the delayed replicas of transmit signal. Such echoes are typically returned from ground, sea, rain, animals/insects which can cause serious performance issues with radar systems n [8]–[12]. In addition to the clutter, there might be radar systems in the vicinity of radar operational regions that illuminate same or similar

electromagnetic waves. In that case, these systems interfere with each other which has not been addressed previously in the literature by using signal separation approach. With this paper, we proposed a signal separation based methods for mitigation of interference created by other radar sources - especially same or similar type- and or radar itself which is known as mutual interference.

The rest of the paper is organized as follows: In Section II, we first define interference mitigation problem as a signal separation problem, briefly review and summarize the state-of-the-art of signal separation. Section-III discuss the selection of appropriate transform domains for sparse representation. The application of the proposed method to the real radar systems is discussed in Section IV. Finally, conclusions are drawn in Section V.

II. SIGNAL SEPARATION FOR INTERFERENCE MITIGATION

Consider the received signal after ADC conversion $\mathbf{y} \in \mathbb{C}^N$ is to be modeled as the sum of multiple component signals, namely signal of interest $\mathbf{y}_r$ and the interference $\mathbf{y}_i$,

$$\mathbf{y} = (\mathbf{y}_r + \mathbf{y}_i) + \mathbf{n}, \tag{1}$$

where $\mathbf{n}$ represent Gaussian noise component. The estimation of different components from received signal can only be meaningfully performed when signal components and the received signal have distinct properties and when these properties are known or approximately known. Furthermore, Signal-to-Noise ratio (SNR) should be high enough to distinguish each signal component itself. In another word, $\mathbf{y}_r$ and $\mathbf{y}_i$ should be sufficiently distinct from $\mathbf{y}$ so as to make the problem meaningful. For simplicity in derivation, we assume SNR is high enough to distinguish each signal components ($\mathbf{n} \simeq 0$ thus $\mathbf{y} = \mathbf{y}_r + \mathbf{y}_i$).

The Morphological Component Analysis (MCA) approach assumes that two component signals allow sparse representations with respect to distinct transforms, $\mathbf{F}_r$ and $\mathbf{F}_i$, respectively [13]. If the component signals are represented in terms of the coefficients, such that

$$\mathbf{y}_r = \mathbf{F}_r\mathbf{a}_r, \quad \mathbf{y}_i = \mathbf{F}_i\mathbf{a}_i. \tag{2}$$

Therefore instead of finding $\mathbf{y}_r$ and $\mathbf{y}_i$ such that $\mathbf{y} = \mathbf{y}_r + \mathbf{y}_i$, we can equivalently find the coefficients $\mathbf{a}_r$ and $\mathbf{a}_i$ in another domain such that

$$\mathbf{y} = \mathbf{F}_r\mathbf{a}_r + \mathbf{F}_i\mathbf{a}_i. \tag{3}$$

Similar to the problem shown in Equation (1), this problem is also ill-conditioned. To find a particular solution, MCA follows a variational framework and minimizes a predetermined cost function chosen to promote sparsity of $\mathbf{a}_r$ and $\mathbf{a}_i$.

To find the optimal coefficients one may consider a ℓ_1-norm approach, which can be shown as

$$\{\hat{\mathbf{a}}_r, \hat{\mathbf{a}}_i\} = \arg\min_{\mathbf{a}_r, \mathbf{a}_i} \lambda_r\|\mathbf{a}_r\|_1 + \lambda_i\|\mathbf{a}_i\|_1 \tag{4a}$$

$$\text{subject to } \mathbf{y} = \mathbf{F}_r\mathbf{a}_r + \mathbf{F}_i\mathbf{a}_i, \tag{4b}$$

where the parameter λ_r and λ_i are positive valued regularization parameters and are used to adjust the trade-off between the two terms. For equal trade off and simplicity, they can be defined as $\lambda_r = \lambda$ and $\lambda_i = (1-\lambda)$. The above problem (4) is a variation of basis pursuit (BP) problem and can only be solved iteratively [14]. Here, the ℓ_1 norm of a vector $\mathbf{x}$ is defined as $\|\mathbf{x}\|_1 = \sum_n |x(n)|$ which promotes sparsity in the optimization problem. The improved results can be obtained by replacing the ℓ_1 norm penalty function by a suitably chosen non-convex penalty functions [15]. Furthermore, when the noise is present, such as in (1), the optimization problem for signal separation turns out a variation of the basis pursuit denoising (BPS) problem [14], which can be written as

$$\{\hat{\mathbf{a}}_r, \hat{\mathbf{a}}_i\} = \arg\min_{\mathbf{a}_r, \mathbf{a}_i} \|\mathbf{y}-\mathbf{F}_r\mathbf{a}_r - \mathbf{F}_i\mathbf{a}_i\|_2^2+\lambda_r\|\mathbf{a}_r\|_1+\lambda_i\|\mathbf{a}_i\|_1. \tag{5}$$

Basis pursuit and basis pursuit denoising can be solved using proximal splitting methods such as Douglas-Rachford approach [16] or split augmented Lagrangian shrinkage algorithm (SALSA) [17] which is based on the alternating direction method of multipliers (ADMM) [18]. In this paper, we use convex ℓ_1 norm penalty functions as regularizer as shown in (4) and used SALSA to achieve optimal coefficients $\hat{\mathbf{a}}_r$ and $\hat{\mathbf{a}}_i$ as shown in Algorithm 1. When the optimal coefficients achieved, the signal of interest is estimated as $\hat{\mathbf{y}}_r = \mathbf{F}_r\hat{\mathbf{a}}_r$.

Algorithm 1 Solution of (4) Using SALSA

Input : $\mathbf{y}$

Initialize: $\mathbf{d}_r \geq 0$, $\mathbf{d}_i \geq 0$ and $\mathbf{F}_r = \text{FT}$, $\mathbf{F}_i = \text{STFT}$

Repeat until converge:

$\mathbf{v}_r \leftarrow soft(\mathbf{a}_r + \mathbf{d}_r, \frac{\lambda}{2\mu}) - \mathbf{d}_r$

$\mathbf{v}_i \leftarrow soft(\mathbf{a}_i + \mathbf{d}_i, \frac{1-\lambda}{2\mu}) - \mathbf{d}_i$

$\mathbf{x} \leftarrow \mathbf{y} - \mathbf{F}_r\mathbf{a}_r - \mathbf{F}_i\mathbf{a}_i$

$\mathbf{d}_r \leftarrow \frac{1}{2}\mathbf{F}_r^H\mathbf{x}$

$\mathbf{d}_i \leftarrow \frac{1}{2}\mathbf{F}_i^H\mathbf{x}$

$\mathbf{a}_r \leftarrow \mathbf{d}_r + \mathbf{v}_r$

$\mathbf{a}_i \leftarrow \mathbf{d}_i + \mathbf{v}_i$

where $soft(\mathbf{z}, T) = \mathbf{z}\,max(0, 1 - T/|z|)$ and $(\bullet)^H$ is the complex conjugate transpose (Hermitian transpose).

The algorithm parameters μ is a positive scalar whose values does not affect the solution to which the algorithm converges, but it does affect the convergence rate.

III. SELECTION OF TRANSFORM DOMAINS

For a successful separation, it is crucial to represent each signal component sparser than the other in a different transform domain. Moreover, each forward and inverse transform pair should preserve total energy (as in Parseval's theorem $\mathbf{F}\mathbf{F}^H = \mathbf{I}$).

Note that the signal of interest is of the form of a sinusoid [7], [19], [20], so it can be sparsely represented in the frequency domain using Fourier transform (FT).

Whereas the Fourier transform of the interference signal is of the form of Fresnel integrals [19], [21]. Due to the fact that, the interference signal is not sparse in the frequency domain. Since the interference signal has a quadratic phase, it can be sparsely represented by time-frequency analysis. Unlike the Fourier transform the short-time Fourier transform (STFT) is suitable for non-stationary signals comprised of time-varying frequency components. It should be noted that signal of interest has sparse like representation in STFT domain. Since the signal of interest is more sparsely represented in the frequency domain using the Fourier transform than in the time-frequency domain using the STFT, MCA is able to recover both signal component successfully.

IV. EXPERIMENTS AND RESULTS

In this section, we demonstrated the application of the proposed method into different radar systems for asynchronous and synchronous interference mitigation. Unlike the traditional methods in literature proposed method does not need to detect and identify the interference thus its novel in terms of application. Instead, it treats interference mitigation problem as a signal separation problem. Thus, when interference is not present results are not affected by the process.

A. ASYNCHRONOUS INTERFERENCE

Application of the proposed method to the automotive radar domain might be a good example for asynchronous interference since automotive radars - especially same brands- have similar system specification (such as bandwidth, carrier frequency, chirp rate, duration...) but random starting time and initial phase. It should be noted that not all pulses are affected by interference. The appearance and duration of the interference depend on different factors such as the slope of the interference, the cut-off frequency of LPF and etc. as discussed in [19].

Case Study 1 (Automotive Radar Interference): We set up an controlled experiment using two MIMO Automotive radar to evaluate the success of the mitigation. A new generation NXP Dolphin T2V2 transceiver chip at a 78.8 GHz center frequency with a bandwidth of 1.0 GHz is set up as the reference automotive radar whereas NXP TEF810X transceiver chip together with S32R274 Radar Microcontroller is used as the interferer car radar.

A moving target (0 dBm^2 at 77 GHz) is located at 5 m range from the reference radar unit. The interferer radar is located at 5 m away from the reference radar unit with a 30° degree offset, which is set to operate with 1 GHz bandwidth at the 78.6 GHz center frequency. Both automotive radar units have 3 transmitters and 4 receivers, thus operate in MIMO mode. Reference radar is set to transmit 256 chirps with a duration of 36.66 μsec per processing frame, whereas interferer radar chirp duration is 40.05 μsec to create asynchronous interference. Samples per chirp for each radar are set to 512 and 256 for reference radar and interferer radar respectively. The specifications of both radars are summarized at Table 1.

TABLE 1. Specification of the reference and the interferer automotive radars.

	Reference Radar	Interferer Radar
Hardware	NXP Dolphin T2V2	NXP TEF810X / S32R274
Bandwidth	∼1 GHz	∼1 GHz
Carrier Frequency	78.8 GHz	78.6 GHz
Samples/Chirp	512	256
Number of Chirps	256	256
Chirp Time	36.66 μsec	40.05 μsec
Mode	MIMO 3TX - 4RX	MIMO 3TX - 4RX

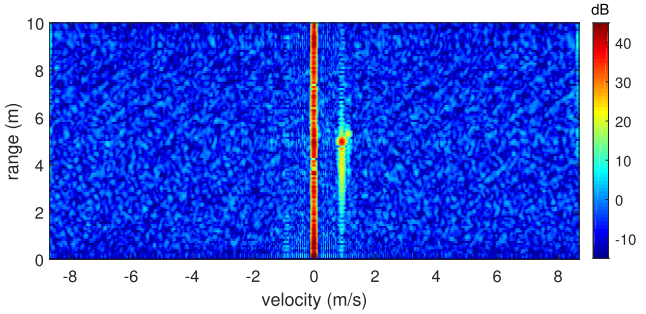

FIGURE 1. Range-Doppler plot of collected signal. Distortion due to the interference is observable as increased noise floor and diagonal streaks.

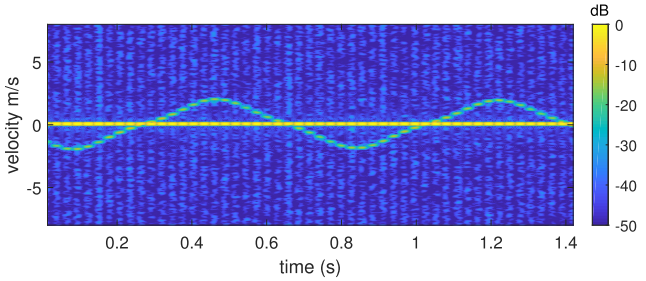

FIGURE 2. STFT of collected signal which is distorted due to the interference. Doppler streaks caused by interference are observable.

Figure 2 shows the STFT of the collected signal for 1.4 seconds of data. The sinusoidal behavior of the controlled target is observable since its velocity varies by time (±2.5 m/s). Distortion due to the interference occurs at different time instances as a streak along Doppler (velocity) axis.

Collected data is also illustrated in range-Doppler (velocity) domain in Figure 1. As seen in the figure, all stationary objects contribute to the ground clutter appear at 0 m/s. Moving pendulum is observed at 5m and 1m/s for the specific time instance. In the range-Doppler domain, the interference appears as diagonal streaks due to the different slope of reference and interferer radar, which causes an overall noise floor increase.

B. SYNCHRONOUS INTERFERENCE

Sometimes interference signal is completely synchronized with the signal of interest such as multiple simultaneous channels operate inside the same radar system. Even though the synchronous operation is supported by orthogonality such as using code division (phase coded waveforms) or polarimetric transmission (Horizontal polarized and Vertically polarized waveforms), in some cases mutual interference is unavoidable due to the imperfect orthogonality of different channels.

Case Study 2 (Parsax Radar): Polarimetric Agile Radar in S- and X-band a.k.a PARSAX is a waveform agile full-polarimetric S-band (3.315 GHz) radar which is operated by Delft University of Technology (TU Delft). The standard deramping processing technique is used to achieve range profiles up to 15 km with a resolution around 3 m [22], [23]. The embedded fast FPGA-based digital processing board with large memory buffer and multiple GPUs in an interconnected PC give the possibility to implement complicated algorithms for signal and data processing. PARSAX use dual-orthogonal (positive and negative frequency excursion) LFM waveforms to realize different polarization channels, thus it suffers from cross-channel mutual interference.

Figure 3 shows beat-frequency versus time graph of a pulse of PARSAX. The cut-off region of the LPF is clearly observable (transition band of LPF spans between 5MHz and 7 MHz). Interference creates a *'V'* shaped signal form exactly in the middle of the pulse where up-chirp and down-chirp signals (positive and negative frequency excursion of LFM waveforms in different polarization channels) are highly overlapped, mixed and pass through the LPF. The other 'V' shaped interferences that are observed on top of the image (above 6 MHz) are due to the mixture of the internal clock (at 135 MHz) of the FPGA with the reference signal. These interferences do not create any distortion since they are out of the beat-frequency band and they can be filtered out easily in the digital domain.

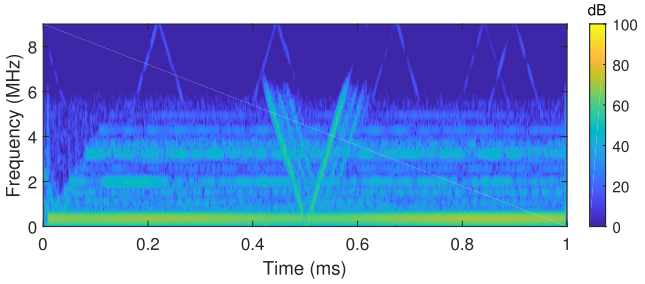

FIGURE 3. Beat-frequency versus time (STFT) of one pulse of PARSAX at HH-channel (Horizontally transmitted - Horizontally received) while simultaneous dual-polarized transmission (H and V). Mutual interference is present in between 0.4 and 0.6 ms.

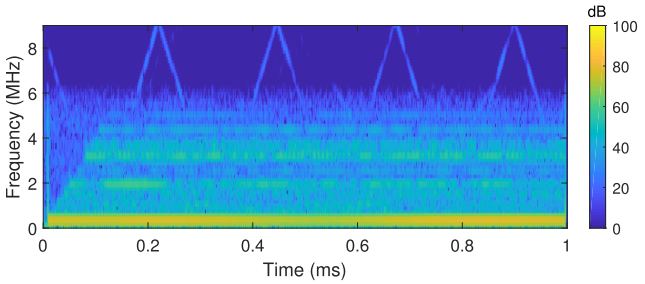

FIGURE 4. Beat-frequency versus time (STFT) of one pulse of PARSAX at HH-channel (Horizontally transmitted - Horizontally received) while single-polarized transmission (only H). Mutual interference due to cross-polarized channel is not present.

As a reference, Figure 4 illustrates a single pulse of PARSAX when only horizontally transmitted and horizontally received channel (HH). Since the vertically polarized channel (V) is set off, there is no mutual interference present in the signal. Note that, similar to asynchronous interference, synchronous interference also causes a noise floor increase in range domain and streaks in the Doppler domain.

C. RESULTS

In this section, we demonstrate the success of the proposed algorithm in mitigating the synchronous and asynchronous interference and discuss the outcomes.

For both cases, SALSA is used (as shown in Algorithm 1) to estimate the sparse coefficients of the signal of interest. We implement a windowed (power-of-sine window) STFT with 75% overlapping for time-frequency domain representation of the signals. Whereas Discrete-time Fourier transform is used for frequency domain representation. The number of iterations is set to 50 for both cases since SALSA usually converges after 15-20 iterations. We set the regularization parameter $\lambda = 0.5$ to penalize the sparsity constraint of each signal component equally.

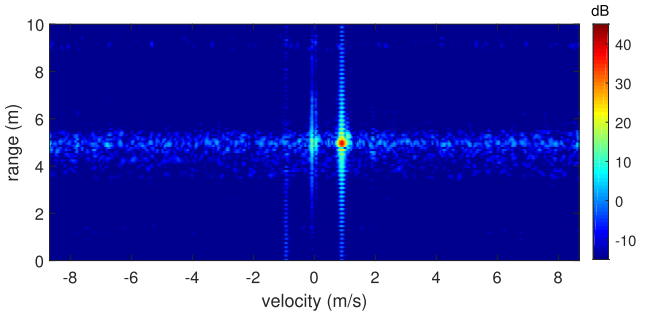

FIGURE 5. Result of automotive radar interference mitigation: Range-Doppler plot of the estimated signal of interest.

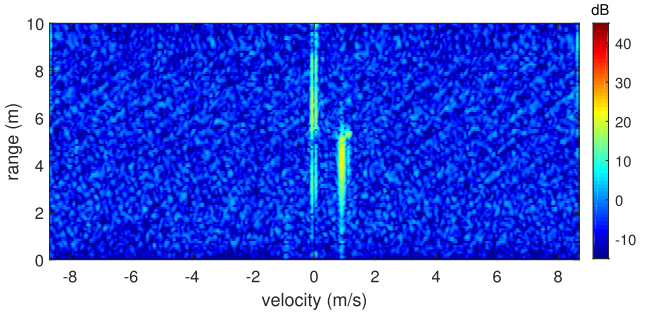

FIGURE 6. Result of automotive radar interference mitigation: Range-Doppler plot of estimated interference component.

1) RESULTS OF CASE STUDY 1

We apply the proposed algorithm to collected automotive radar data to mitigate the asynchronous interference created another radar in the vicinity of the reference radar's operational region. As a preprocessing, a ground clutter filter (GCF) is applied to the collected radar data to concentrate on only moving targets.

Estimated two signal components are illustrated in Figure 7 and Figure 8 for signal of interest and the inter-

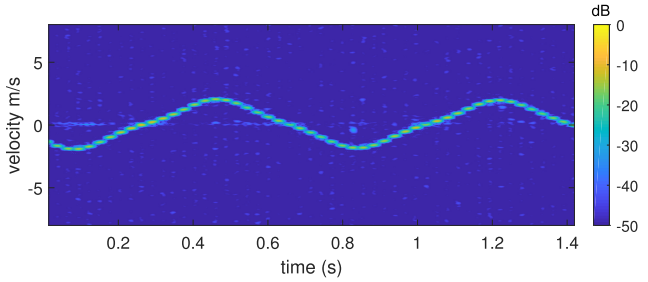

FIGURE 7. Result of automotive radar interference mitigation: STFT of estimated signal of interest after signal separation.

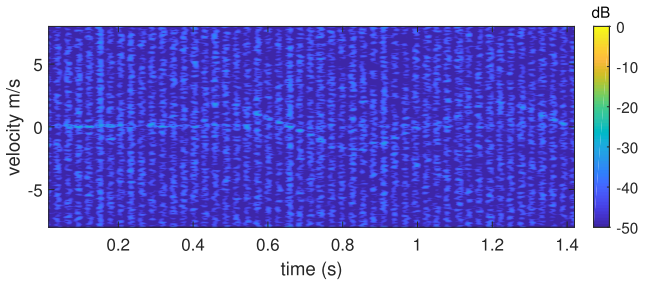

FIGURE 8. Result of automotive radar interference mitigation: STFT of estimated interference signal after signal separation. Some residual from signal of interest are still present.

ference signal, respectively. As seen from the figures, proposed algorithm successfully separate two signal component. In Figure 8, some residuals from signal of interest are observable. It should be noted that residuals can be reduced and the overall result can be improved by changing the λ value.

Same results are also illustrated in the range-Doppler domain to demonstrate the effect of interference mitigation in Doppler processing. Figure 5 and Figure 6 show the range-Doppler plot of signal of interest and the interference signal, respectively. As a result, the high noise floor and the diagonal streaks due to the interference successfully separated from the signal of interest.

Bear in mind that in automotive radar the interference sometimes caused by a CW radar but not FMCW radar as presented in this paper. Our experiments show that the proposed method can successfully mitigate CW interference as well. The detailed investigation of the CW interference on an FMCW automotive radar system is discussed at [19].

2) RESULTS OF CASE STUDY 2

In this section, we present the results of the proposed approach for synchronous interference mitigation, especially for mutual interference. Unlike an automotive radar PARSAX is agiler and allows us to collect more samples thus we can achieve better time-frequency representation of the interference signal. STFT of the estimated interference signal is illustrated in Figure 9. Even though there are some residuals from beat-frequencies at the beginning and the end portion of the pulse, the signal separation is successful. Note that the beginning and the end portion of the FMCW pulses are usually not used for processing, thus the loss in the signal at that regions does not affect the final results (such as range estimates). Similarly, Figure 10 illustrates the estimated beat frequencies.

Unlike the previous example (automotive radar case), this time we concentrate on the stationary target. Thus we further processed beat-frequencies to achieve range information of stationary targets. Figure 11 shows the range profile of three different signals; Namely, the signal that is distorted by interference (blue line), signal after interference mitigation (red line) and as a reference undistorted signal (orange) which collected by setting off the vertically polarized channel. As seen from the figure, the distorted signal has a high noise floor due to the mutual interference which masks the small RCS targets in far range.

To explore the success of the signal separation algorithm, a zoomed version of Figure 11 is illustrated in Figure 12 which shows a range between 5.1 to 5.6 km. A common trend is observable between interference mitigated signal (red) and interference-free signal (orange). Both signals make similar peaks at around possible targets (such as the one at ~ 5.18 km), whereas their sidelobe behavior show differences due to scintillation of the returned waveform from pulse-to-pulse. It should be noted that without proposed interference mitigation, it is not possible to detect such weak targets in the synchronous dual-polarization mode. In range-Doppler imaging at PARSAX similar effects -like in automotive radar case- are observed and successfully mitigated using the proposed method.

D. IMPROVEMENT IN SIGNAL-TO-INTERFERENCE RATIO (SIR)

It is hard to define exact improvement in the signal-to-interference ratio for an asynchronous interference since

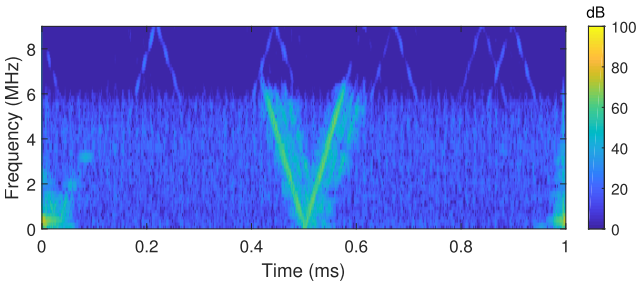

FIGURE 9. Result of mutual interference mitigation: STFT of estimated interference signal after signal separation.

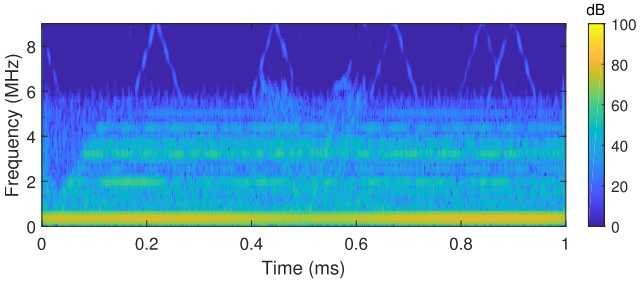

FIGURE 10. Result of mutual interference mitigation: STFT of estimated signal of interest (beat-frequencies) after signal separation.

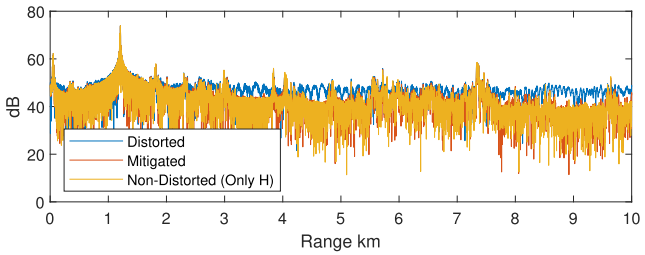

FIGURE 11. Result of mutual interference mitigation: Comparison of range profiles before and after mitigation. H only transmission is given as reference.

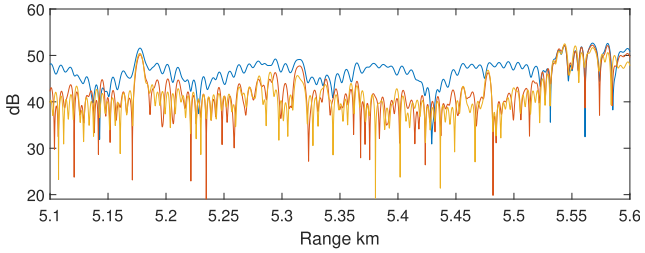

FIGURE 12. Result of mutual interference mitigation: detailed investigation (zoomed version) of figure 12.

the duration of the interference changes by time which depends on different parameters, especially to the time delay of the interferer with respect to initial time of transmitted chirp. Experiments show that asynchronous interference appears different time instances with different durations inside each pulse due to the different system parameters which summarized in Table-1.

In practice, it is not possible to determine exact duration of the interference (unless the exact transfer function of the system is known) since different low-pass filters may have different transition bands and ringing effects on the signals. Due to the fact that, for this particular example signal to interference ratio computed manually only for the samples where the interference present in the time domain signal (which is selected manually from the figure). In that particular region, SIR is computed -11.85 dB. Note that, the interference signal y_i is only present for a limited time region and may only affect some of the samples [19]. In this particular frame (shown in Figure 1), which consists of 256 slow-time (pulse) and 512 fast-time samples, only 7 out of 256 pulses were distorted by asynchronous interference where overall 12dB gain observed after application of the proposed method.

PARSAX suffers from synchronous interference which is present for all received pulses (duration of the interference and affected samples within a pulse are known and always same). Similarly, in PARSAX radar a 10.5 dB gain observed in time domain SIR. As we have discussed in Section IV, this improvement helps to exploit weaker targets masked due to the mutual interference like in Figure 12).

V. CONCLUSION

This letter has applied classical signal separation approach to radar data sets to address the synchronous and asynchronous interference mitigation problem. The effect of the interference into the different radar products (such as range, range-Doppler) are demonstrated and discussed with details. We propose appropriate transform domains where interference and signal of interest can be sparsely represented so that SALSA algorithm can be used to execute the signal separation for interference mitigation.

We address the questions regarding the broad applicability of the proposed method since the success of the proposed algorithm is shown in different cases without any specific modification. Overall, in asynchronous and synchronous interference, significant improvement is observed in signal to interference ratio after the application of the proposed method, which yields successful detection of the weaker targets that are masked by the interference.

The current implementation of the algorithm can be applicable to large-sized systems such as PARSAX radar for real-time processing due to the necessary computational load. However, an efficient implementation of the algorithm in real-time systems and low SNR cases (where the signal of interest can be barely represented as sparse) are still open as future works.

ACKNOWLEDGMENT

The authors would like to thank Oleg Krasnov and Sharef Neemat at Delft University of Technology for their valuable discussion during the processing of PARSAX data, also Pascal J. Aubry for his help during the automotive radar experiments. They gratefully acknowledge the hardware support from NXP Semiconductors N.V. Netherlands.

REFERENCES

[1] G. Fabrizio and A. Farina, "Blind source separation with the generalised estimation of multipath signals algorithm," *IET Radar, Sonar Navigat.*, vol. 8, no. 9, pp. 1255–1266, 2014.

[2] J. Li, R. Wu, Y. Hao, X. Wang, Y. Wang, and A. Zhao, "DME interference suppression algorithm based on signal separation estimation theory for civil aviation system," *EURASIP J. Wireless Commun. Netw.*, vol. 2016, no. 1, p. 247, Oct. 2016, doi: 10.1186/s13638-016-0736-8.

[3] M. Tao, F. Zhou, J. Liu, Z. Zhang, and Z. Bao, "Narrow-band interference mitigation for SAR using independent subspace analysis," *IEEE Trans. Geosci. Remote Sens.*, vol. 52, no. 9, pp. 5289–5301, Sep. 2014.

[4] B. Osmanoglu, R. Rincon, S. Lee, T. Fatoyinbo, and T. Bollian, "Radio frequency interference detection and mitigation techniques using data from EcoSAR 2014 flight campaign," in *Proc. IEEE Int. Geosci. Remote Sens. Symp. (IGARSS)*, Jul. 2015, pp. 124–127.

[5] M. Kunert, "The EU project MOSARIM: A general overview of project objectives and conducted work," in *Proc. 9th Eur. Radar Conf.*, Oct./Nov. 2012, pp. 1–5.

[6] M. Barjenbruch, D. Kellner, K. Dietmayer, J. Klappstein, and J. Dickmann, "A method for interference cancellation in automotive radar," in *Proc. IEEE MTT-S Int. Conf. Microw. Intell. Mobility (ICMIM)*, Apr. 2015, pp. 1–4.

[7] J. Bechter, F. Roos, M. Rahman, and C. Waldschmidt, "Automotive radar interference mitigation using a sparse sampling approach," in *Proc. Eur. Radar Conf. (EuRAD)*, Oct. 2017, pp. 90–93.

[8] I. W. Selesnick, K. Y. Li, S. U. Pillai, and B. Himed, "Doppler-streak attenuation via oscillatory-plus-transient decomposition of IQ data," in *Proc. IET Int. Conf. Radar Syst. (Radar)*, Oct. 2012, pp. 1–4.

[9] F. Uysal, I. Selesnick, U. Pillai, and B. Himed, "Dynamic clutter mitigation using sparse optimization," *IEEE Aerosp. Electron. Syst. Mag.*, vol. 29, no. 7, pp. 37–49, Jul. 2014.

[10] F. Uysal, I. Selesnick, and B. M. Isom, "Mitigation of wind turbine clutter for weather radar by signal separation," *IEEE Trans. Geosci. Remote Sens.*, vol. 54, no. 5, pp. 2925–2934, May 2016.

[11] B. Ng, L. Rosenberg, and S. T. N. Nguyen, "Target detection in sea clutter using resonance based signal decomposition," in *Proc. IEEE Radar Conf. (RadarConf)*, May 2016, pp. 1–6.
[12] M. Farshchian, "Target extraction and imaging of maritime targets in the sea clutter spectrum using sparse separation," *IEEE Geosci. Remote Sens. Lett.*, vol. 14, no. 2, pp. 232–236, Feb. 2017.
[13] J.-L. Starck, Y. Moudden, J. Bobin, M. Elad, and D. L. Donoho, "Morphological component analysis," *Proc. SPIE*, vol. 5914, pp. 5914-1–5914-15, Sep. 2005, doi: 10.1117/12.615237.
[14] S. S. Chen, D. L. Donoho, and M. A. Saunders, "Atomic decomposition by basis pursuit," *SIAM J. Sci. Comput.*, vol. 20, no. 1, pp. 33–61, 1999, doi: 10.1137/S1064827596304010.
[15] I. Selesnick and M. Farshchian, "Sparse signal approximation via nonseparable regularization," *IEEE Trans. Signal Process.*, vol. 65, no. 10, pp. 2561–2575, May 2017.
[16] J. Eckstein and D. P. Bertsekas, "On the Douglas–Rachford splitting method and the proximal point algorithm for maximal monotone operators," *Math. Program.*, vol. 55, nos. 1–3, pp. 293–318, 1992.
[17] M. V. Afonso, J.-M. Bioucas-Dias, and M. A. T. Figueiredo, "Fast image recovery using variable splitting and constrained optimization," *IEEE Trans. Image Process.*, vol. 19, no. 9, pp. 2345–2356, Sep. 2010.
[18] S. Boyd, N. Parikh, E. Chu, B. Peleato, and J. Eckstein, "Distributed optimization and statistical learning via the alternating direction method of multipliers," *Found. Trends Mach. Learn.*, vol. 3, no. 1, pp. 1–122, Jan. 2011.
[19] F. Uysal and S. Sanka, "Mitigation of automotive radar interference," in *Proc. IEEE Radar Conf.*, Apr. 2018, pp. 405–410.
[20] T. Schipper, T. Mahler, M. Harter, L. Reichardt, and T. Zwick, "An estimation of the operating range for frequency modulated radars in the presence of interference," in *Proc. Eur. Radar Conf.*, Oct. 2013, pp. 227–230.
[21] M. Jankiraman, *Design of Multi-frequency CW Radars*, vol. 2. West Perth, PA, Australia: SciTech Publishing, 2007.
[22] O. A. Krasnov, L. P. Ligthart, Z. Li, P. Lys, and F. van der Zwan, "The PARSAX—Full polarimetric FMCW radar with dual-orthogonal signals," in *Proc. Eur. Radar Conf.*, Oct. 2008, pp. 84–87.
[23] O. A. Krasnov, G. P. Babur, L. P. Ligthart, and F. van der Zwan, "Basics and first experiments demonstrating isolation improvements in the agile polarimetric FM-CW radar; PARSAX," in *Proc. Eur. Radar Conf. (EuRAD)*, Sep. 2009, pp. 13–16.

FARUK UYSAL (M'07–SM'16) received the M.S. and Ph.D. degrees in electrical engineering from New York University, NY, USA, in 2010 and 2016, respectively. During his study, he focused on signal separation techniques for dynamic clutter mitigation. From 2011 to 2014, he was a Staff Engineer at C&P Technologies, Inc., Closter, NJ, USA. He was a Radar Engineer with the Advanced Radar Research Center (ARRC), The University of Oklahoma, Norman, OK, USA, from 2014 to 2016, where he was involved in the design and implementation of various projects from the U.S. Department of Defense agencies.

In 2016, he joined the Microwave Sensing, Signals and Systems Section, Faculty of Electrical Engineering, Mathematics, and Computer Science, Delft University of Technology, as an Assistant Professor. He is responsible for the research in the field of distributed radar networks and automotive radar. His current research interests include radar signal processing, waveform design, beamforming, radar image formation, clutter mitigation, and cognitive radar.

Dr. Uysal is a Member of URSI and an Affiliate Member of ARRC, The University of Oklahoma.